# Iron(II) Polyamine Chemistry: Variation of Spin State and Coordination Number in Solid State and Solution with Iron(II) Tris(2-pyridylmethyl)amine Complexes

**Alain Diebold and Karl S. Hagen***

Department of Chemistry, Emory University, Atlanta, Georgia 30322

*Received August 29, 1997*

The synthetic system of $Fe(SO_3CF_3)_2$ and one or two TPA ligands (TPA = tris(2-pyridylmethyl)amine) affords a series of complexes that demonstrate the complexities of the solid-state and solution coordination chemistry of labile iron(II) even with a multidentate ligand. The low-spin $[Fe(TPA)(CH_3CN)_2](SO_3CF_3)_2$ (**1**-OTf) complex forms in acetonitrile, but the high-spin complex $Fe(TPA)(SO_3CF_3)_2$ (**2**) forms in chloroform. The methanol-bound complex $[Fe(TPA)(CH_3OH)_2](BPh_4)_2$ (**3**) forms in the presence of the noncoordinating anion, $BPh_4^-$, and six-coordinate $[Fe(TPA)_2](SO_3CF_3)_2$ (**4**-OTf) and eight-coordinate $[Fe(TPA)_2](BPh_4)_2$ (**4**-$BPh_4$) form in the presence of excess ligand. Their behavior in solution is explored by studying their magnetic properties and NMR spectra, which indicate the presence of spin and coordination equilibria. The crystal structures of these complexes are reported. Crystallographic parameters are as follows. **1**-OTf·$CH_3CN$: $C_{26}H_{27}F_6FeN_7O_6S_2$, monoclinic, $P2_1/n$, $a$ = 12.418(2) Å, $b$ = 16.192(4) Å, $c$ = 15.855(2) Å, $\beta$ = 92.09(2)°, $Z$ = 4. **2**: $C_{20}H_{18}F_6FeN_4O_6S_2$, monoclinic, $P2_1/c$, $a$ = 17.636(2) Å, $b$ = 9.659(1) Å, $c$ = 16.004(2) Å, $\beta$ = 113.29 (1)°, $Z$ = 4. **3**·$CH_3OH$: $C_{69}H_{70}B_2FeN_4O_3$, monoclinic, $P2_1/n$, $a$ = 17.525(1) Å, $b$ = 19.150(2) Å, $c$ = 17.703(1) Å, $\beta$ = 100.36(1)°, $Z$ = 4. **4**-OTf: $C_{38}H_{36}F_6FeN_8O_6S_2$, monoclinic, $Pc$, $a$ = 10.236(1) Å, $b$ = 10.129(1) Å, $c$ = 19.251(1) Å, $\beta$ = 92.27(1)°, $Z$ = 2. **4**-$BPh_4$: $C_{84}H_{76}B_2FeN_8$, monoclinic, $P2_1/n$, $a$ = 12.489(1) Å, $b$ = 14.189(1) Å, $c$ = 19.843(1) Å, $\beta$ = 102.84(1)°, $Z$ = 2.

## Introduction

Synthetic model studies of the active sites of metalloproteins that involve imidazole have utilized a number of polydentate amine ligands in order to form stable complexes.[1] Non-heme iron proteins are such a class, and the reduced forms of these proteins generally exist as HS iron(II). The polydentate nature of these ligands makes the isolation of iron(II) complexes, which are generally very labile, tractable. However, a complicating feature of these amine ligands is that they can form either low-spin ($^1A_1$, LS), high-spin ($^5T_2$, HS), six-coordinate iron(II) complexes or complexes that exhibit a temperature-, light-, or pressure-induced LS ↔ HS transition. This is an active area of research that has been extensively reviewed.[2−8] Most of these studies have been carried out in the solid state whereas we are concerned with understanding the behavior of these labile iron(II) complexes in solution.

The extremes of ligand types are the simple aliphatic amines and pyridine type imines. Of these, the homoleptic monodentate complexes $[Fe(NH_3)_6]^{2+}$ [9] and $[Fe(py)_6]^{2+}$ [10] are both HS as is the tris chelate $[Fe(en)_3]^{2+}$,[11] whereas $[Fe(bipy)_3]^{2+}$ and $[Fe(phen)_3]^{2+}$ [12] are each stable, diamagnetic, LS complexes. However, addition of one methyl substituent on the phen[13] and bipy[14] ligands causes the electron configuration of the iron(II) complexes to switch to LS ↔ HS, and two methyl substituents on phen cause it to remain HS even at low temperatures.[15] A mixture of one aliphatic amine and one pyridine, as in 2-(aminomethyl)pyridine (2-pic), affords either the LS *fac* isomer or *mer* isomers that are either LS ($[Fe(2\text{-pic})_3]Cl_2\cdot 2H_2O$) or LS ↔ HS for other solvates.[16−18]

The tridentate ligand dien forms a HS complex, $[Fe(dien)_2]^{2+}$;[19] however, the macrocycle tacn affords a complex, $[Fe(tacn)_2]^{2+}$, that is LS in the solid state[20] but exhibits LS ↔ HS behavior in solution.[19] The pyridine-containing ligand bis-

(1) (a) Wieghardt, K. *Angew. Chem., Int. Ed. Engl.* **1989**, *28*, 1153−1172. (b) Lippard, S. J. *Angew. Chem., Int. Ed. Engl.* **1988**, *27*, 344−361.
(2) Goodwin, H. A. *Coord. Chem. Rev.* **1976**, *18*, 293−325.
(3) Toftlund, H. *Coord. Chem. Rev.* **1989**, *94*, 67−108.
(4) Gütlich, P. *Struct. Bonding* **1981**, *44*, 83−195.
(5) Gütlich, P.; Hauser, A. *Coord. Chem. Rev.* **1990**, *97*, 1−22.
(6) König, E. *Struct. Bonding* **1991**, *76*, 51−152.
(7) Hauser, A. *Coord. Chem. Rev.* **1991**, *111*, 275−290.
(8) Gütlich, P.; Hauser, A.; Spiering, H. *Angew. Chem., Int. Ed. Engl.* **1994**, *33*, 2024−2054.
(9) (a) Schmidt, K. H.; Müller, A. *Inorg. Chem.* **1975**, *14*, 2183−2187. (b) Asch, L.; Shenoy, G. K.; Friedt, J. M.; Adloff, J. P. *J. Chem. Phys.* **1975**, *62*, 2335−2342.
(10) Doedens, R. J.; Dahl, L. F. *J. Am. Chem. Soc.* **1966**, *88*, 4847−4855.
(11) Nair, V. S. Ph.D. Thesis, Emory University, Atlanta, GA, 1996.
(12) Irving, H.; Mellor, D. H. *J. Chem. Soc.* **1962**, 5237−5245.
(13) (a) Goodwin, H. A.; Sylva, R. N. *Aust. J. Chem.* **1968**, *21*, 83−90. (b) König, E.; Ritter, G.; Spiering, H.; Kremer, S.; Madeja, K.; Rosenkranz, A. *J. Chem. Phys.* **1972**, *56*, 3139−3145. (c) König, E.; Ritter, G.; Braunecker, B.; Madeja, K.; Goodwin, H. A.; Smith, F. E. *Ber. Bunsen-Ges. Phys. Chem.* **1972**, *76*, 393−400. (d) Fleisch, J.; Gütlich, P.; Hasselbach, K. M.; Müller, W. *Inorg. Chem.* **1976**, *15*, 958−961. (e) König, E.; Ritter, G.; Goodwin, H. A. *J. Inorg. Nucl. Chem.* **1977**, *39*, 1773−1777. (f) Goodwin, H. A.; Kucharski, E. S.; White, A. H. *Aust. J. Chem.* **1983**, *36*, 1115−1124.
(14) Onggo, D.; Hook, J. M.; Rae, A. D.; Goodwin, H. A. *Inorg. Chim. Acta* **1990**, *173*, 19−30.
(15) Fleisch, J.; Gütlich, P.; Hasselbach, K. M.; Müller, W. *J. Phys. (Paris)* **1974**, *35*, C6−159.
(16) (a) Greenaway, A. M.; Sinn, E. *J. Am. Chem. Soc.* **1978**, *100*, 8080−8084. (b) Greenaway, A. M.; O'Connor, C. J.; Schrock, A.; Sinn, E. *Inorg. Chem.* **1979**, *18*, 2692−2695.
(17) (a) Katz, B. A.; Strouse, C. E. *J. Am. Chem. Soc.* **1979**, *101*, 6214−6221. (b) Katz, B. A.; Strouse, C. E. *Inorg. Chem.* **1980**, *19*, 658−665.
(18) Sorai, M.; Ensling, J.; Hasselbach, K. M.; Gütlich, P. *Chem. Phys.* **1977**, *20*, 197−208.
(19) Hagen, K. S. Unpublished.

S0020-1669(97)01105-1 CCC: $15.00 
Published on Web 01/26/1998

(2-pyridylmethyl)amine (dpma) forms a LS complex, $[Fe(dpma)_2]^{2+}$, whereas the methyl-substituted ligand bis(2-pyridylmethyl)methylamine (Medpma) forms a HS complex, $[Fe(Medpma)_2]^{2+}$.[21] Both the *fac* complex with the tripyridine ligand, tris(2-pyridylamine) $[Fe((py)_3N)_2]^{2+}$,[22] and the *mer* complex of the terpyridine ligand, $[Fe(terpy)_2]^{2+}$,[23] are LS at room temperature. The tripodal tetradentate ligand tris(2-aminoethyl)amine (tren) readily forms a HS six-coordinate complex, $[Fe(tren)_2]^{2+}$, in which one arm from each ligand is not coordinated.[19] The analogous pyridine-containing ligand, tris(2-pyridylmethyl)amine (TPA), has been widely used in studies of LS ↔ HS behavior in iron(II) complexes (in which the remaining two coordination sites are occupied by good donor ligands)[3] and in model complexes of non-heme iron proteins.[24]

We describe here a series of complexes formed between iron(II) triflate and tris(2-pyridylmethyl)amine (TPA) in which the stoichiometry, the solvent, and the counterion can effectively control the coordination number and spin state of the complexes in solution and in the solid state. Structural, associated spectroscopic, and other physical properties are presented.

## Experimental Section

**Materials.** Reagents and solvents used were of commercially available reagent quality unless otherwise stated. Methanol and chloroform were distilled from $CaH_2$. Deoxygenation of solvents was effected by bubbling $N_2$ directly through the solutions. Preparation and handling of air-sensitive materials were performed under an inert atmosphere of $N_2$ in a glovebox. $Fe(SO_3CF_3)_2{\cdot}2CH_3CN$ was prepared by reacting Fe metal and triflic acid in acetonitrile and crystallizing the product by adding diethyl ether. Tris(2-pyridylmethyl)amine (TPA) was synthesized according to a literature procedure.[25]

**Physical Measurements.** Elemental analyses were performed by Atlantic Microlabs, Inc., Atlanta, GA. $^1$H NMR spectra were recorded on a General Electric QE-300, a Nicolet NT-360, a Varian Inova 400, or a General Electric GN-500 spectrometer in $CD_3CN$, $(CD_3)_2CO$, or $CDCl_3$ and referenced to tetramethylsilane. Electronic absorption spectra were collected on a Shimadzu UV-3101PC UV−vis−NIR scanning spectrophotometer. Room-temperature magnetic moments of powder samples were measured using an Evans magnetic susceptibility balance (Johnson Matthey, Model No. MSB-1) using Pascal's constants for diamagnetic corrections, on an instrument calibrated with $Hg[Co(SCN)_4]$. Magnetic moments in solution were measured using the Evans method on either the 300 MHz or the 500 MHz NMR spectrometer.[26]

**$[Fe^{II}(TPA)(CH_3CN)_2](SO_3CF_3)_2$ (1-OTf).** A colorless solution of $Fe(SO_3CF_3)_2{\cdot}2CH_3CN$ (0.44 g, 1.0 mmol) in $CH_3CN$ (2 mL) was added to a solution of TPA (0.29 g, 1.0 mmol) in $CH_3CN$ (2 mL), affording a clear dark red solution. The reaction mixture was stirred for 30 min at room temperature, followed by precipitation with diethyl ether (10 mL) at −30 °C. This procedure led to the isolation of 0.64 g (88%) of the title compound as a microcrystalline red solid. Red crystals of **1**-OTf·$CH_3CN$ suitable for X-ray diffraction analysis were grown at −30 °C by slow diffusion of $Et_2O$ into a dilute $CH_3CN$ solution of **1**-OTf. $^1$H NMR ($CD_3CN$, 360 MHz): $\delta$ 12.12 (br s, 3H, $H_{\alpha(pyr)}$), 9.02 (s, 3H, $H_{\beta/\beta'(pyr)}$), 8.92 (s, 3H, $H_{\beta'/\beta(pyr)}$), 7.33 (t, $J$ = 7.3 Hz, 3H, $H_{\gamma(pyr)}$), 7.09 (s, 6H, $CH_2$). Anal. Calcd for $C_{24}H_{24}N_6F_6FeO_6S_2$: C, 39.68; H, 3.33; N, 11.57. Found: C, 38.83; H, 3.50; N, 11.08. **1**-OTf loses bound $CH_3CN$ under vacuum. Anal. Calcd for $[Fe(TPA)(CH_3CN)_{1.5}](SO_3CF_3)_2$: C, 39.13; H, 3.21; N, 10.91.

**$[Fe^{II}(TPA)(CH_3CN)_2](BPh_4)_2$ (1-$BPh_4$).** Solid **3** (0.97 g, 0.86 mmol; prepared as described below) was dissolved in $CH_3CN$ (3 mL), yielding a dark red solution. Addition of diethyl ether (10 mL), followed by cooling to −30 °C overnight, resulted in the isolation of 0.85 g (92%) of a dark red powder. Red crystals of **1**-$BPh_4$ suitable for X-ray diffraction analysis were grown at −30 °C by slow diffusion of $Et_2O$ into an $CH_3CN$ solution of **1**-$BPh_4$. $^1$H NMR ($CD_3CN$, 300 MHz): $\delta$ 10.91 (br s, 3H, $H_{\alpha(pyr)}$), 8.42−8.39 (br m, 6H, $H_{\beta+\beta'(pyr)}$), 7.20−6.83 (m, 43H, $BPh_4$ + $H_{\gamma(pyr)}$), 6.26 (br s, 6H, $CH_2$). Anal. Calcd for $C_{70}H_{64}N_6B_2Fe$: C, 78.81; H, 6.05; N, 7.88. Found: C, 78.85; H, 6.13; N, 7.83.

**$Fe^{II}(TPA)(SO_3CF_3)_2$ (2).** All of the red solid of **1**-OTf from a 1.0 mmol scale preparation as described above was dissolved in $CHCl_3$ (4 mL), yielding a yellow-orange solution. Precipitation with pentane (10 mL) resulted in the isolation of 0.57 g (88%) of a yellow-orange powder. Yellow crystals of **2** suitable for X-ray diffraction analysis were grown by slow diffusion of pentane into a $CHCl_3$ solution of **2**. $^1$H NMR ($CDCl_3$, 300 MHz): $\delta$ 133.83 (br s, 3H, $H_{\alpha(pyr)}$), 62.12 (br s, 6H, $CH_2$), 51.97 (s, 3H, $H_{\beta/\beta'(pyr)}$), 49.91 (s, 3H, $H_{\beta'/\beta(pyr)}$), 13.40 (s, 3H, $H_{\gamma(pyr)}$). Anal. Calcd for $C_{20}H_{18}N_4F_6FeO_6S_2$: C, 37.28; H, 2.82; N, 8.70. Found: C, 36.61; H, 2.93; N, 8.49.

**$[Fe^{II}(TPA)(CH_3OH)_2](BPh_4)_2$ (3).** A solution of $Fe(SO_3CF_3)_2{\cdot}2CH_3CN$ (0.44 g, 1.0 mmol) in $CH_3OH$ (2 mL) was added to a solution of TPA (0.29 g, 1.0 mmol) in $CH_3OH$ (2 mL), leading to a clear orange solution. The reaction mixture was stirred for 30 min at room temperature, after which a solution of $NaBPh_4$ (0.76 g, 2.2 mmol) in $CH_3OH$ (6 mL) was slowly added. A pale yellow precipitate appeared immediately, which was filtered off and washed with $CH_3OH$. Drying *in vacuo* yielded 0.97 g (86%) of the title compound as a yellow powder. Yellow crystals of **3**·$CH_3OH$ suitable for X-ray diffraction analysis were grown by slow diffusion of pentane into a $CH_3OH$ solution of **3**. $^1$H NMR ($(CD_3)_2CO$, 300 MHz): $\delta$ 123.51 (br s, 3H, $H_{\alpha(pyr)}$), 69.35 (br s, 6H, $CH_2$), 54.78 (s, 3H, $H_{\beta/\beta'(pyr)}$), 53.51 (s, 3H, $H_{\beta'/\beta(pyr)}$), 7.30−6.75 (m, 40H, $BPh_4$), 5.54 (s, 3H, $H_{\gamma(pyr)}$). Anal. Calcd for $C_{71}H_{73}N_5B_2FeO_3$: C, 76.01; H, 6.56; N, 6.24. Found: C, 76.62; H, 6.35; N, 6.25.

**$[Fe^{II}(TPA)_2](SO_3CF_3)_2$ (4-OTf).** A colorless solution of $Fe(SO_3CF_3)_2{\cdot}2CH_3CN$ (0.22 g, 0.5 mmol) in acetone (3 mL) was added to a solution of TPA (0.29 g, 1.0 mmol) in acetone (3 mL), leading to a clear yellow-orange solution. The reaction mixture was stirred for 30 min at room temperature, before the acetone was removed under vacuum, yielding a yellow-orange powder. Light yellow crystals of **4**-OTf suitable for X-ray diffraction analysis were obtained from a yellow oil by slow diffusion of pentane into an acetone solution of **4**-OTf. These crystals were picked out individually using a Pasteur pipet; one of these was used for the X-ray crystal determination, and the others were dried under vacuum, yielding 30 mg (6%) of a light yellow powder. $^1$H NMR ($(CD_3)_2CO$, 300 MHz): $\delta$ 73.83 (br s, 6H, $H_{\alpha(pyr)}$), 41.26 (br s, 12H, $H_{\beta+\beta'(pyr)}$), 30.59 (br s, 12H, $CH_2$).

**$[Fe^{II}(TPA)_2](BPh_4)_2$ (4-$BPh_4$).** A colorless solution of $Fe(SO_3CF_3)_2{\cdot}2CH_3CN$ (0.22 g, 0.5 mmol) in $CH_3OH$ (3 mL) was added to a solution of TPA (0.29 g, 1.0 mmol) in $CH_3OH$ (3 mL), leading to a clear orange solution. The reaction mixture was stirred for 30 min at room temperature, after which a solution of $NaBPh_4$ (0.38 g, 1.1 mmol) in $CH_3OH$ (4 mL) was slowly added. A pale yellow precipitate appeared immediately, which was filtered off and washed with $CH_3OH$. Drying *in vacuo* yielded 0.51 g (80%) of the title compound as a pale yellow powder. Colorless crystals of **4**-$BPh_4$ suitable for X-ray diffraction analysis were grown by slow diffusion of pentane into an acetone solution of **4**-$BPh_4$. $^1$H NMR ($(CD_3)_2CO$, 500 MHz): $\delta$ 74.48 (br s, 6H, $H_{\alpha(pyr)}$), 41.75 (br s, 12H, $H_{\beta+\beta'(pyr)}$), 30.53 (br s, 12H, $CH_2$), 7.39 (s, 16H, $BPh_4$), 6.91 (s, 16H, $BPh_4$), 6.73 (s, 8H, $BPh_4$), 0.29 (br s, 6H, $H_{\gamma(pyr)}$). Anal. Calcd for $C_{84}H_{76}N_8B_2Fe$: C, 79.13; H, 6.01; N, 8.79. Found: C, 79.02; H, 6.03; N, 8.69.

**Crystallographic Studies.** Crystals of **1**-OTf·$CH_3CN$, **1**-$BPh_4$, **2**, **3**·$CH_3OH$, **4**-OTf, and **4**-$BPh_4$ suitable for X-ray crystallographic analysis were obtained as described in the Experimental Section (*vide supra*). All crystals were coated with a viscous oil and mounted with

(20) Boeyens, J. C. A.; Forbes, A. G. S.; Hancock, R. D.; Wieghardt, K. *Inorg. Chem.* **1985**, *24*, 2926−2931.
(21) Nelson, S. M.; Rodgers, J. *J. Chem. Soc. A* **1968**, 272−276.
(22) (a) McWhinnie, W. R.; Poller, R. C.; Thevarasa, M. *J. Chem. Soc. A* **1967**, 1671−1674. (b) Kucharski, E. S.; McWhinnie, W. R.; White, A. H. *Aust. J. Chem.* **1978**, 1671.
(23) (a) Brandt, W. W.; Wright, J. P. *J. Am. Chem. Soc.* **1954**, *76*, 3082−3083. (b) Hogg, R.; Wilkins, R. G. *J. Chem. Soc.* **1962**, 341−350.
(24) Que, L., Jr.; Dong, Y. H. *Acc. Chem. Res.* **1996**, *29*, 190−196.
(25) Tyeklar, Z.; Jacobson, R. R.; Wei, N.; Murthy, N. N.; Zubieta, J.; Karlin, K. D. *J. Am. Chem. Soc*. **1993**, *115*, 2677−2689.
(26) Evans, D. F. *J. Chem. Soc*. **1959**, 2003−2005.

**Table 1.** Crystallographic Data for the Iron(II) TPA Complexes

| | **1**-OTf·$CH_3CN$ | **2** | **3**·$CH_3OH$ | **4**-OTf | **4**-$BPh_4$ |
|---|---|---|---|---|---|
| empirical formula | $C_{26}H_{27}F_6FeN_7O_6S_2$ | $C_{20}H_{18}F_6FeN_4O_6S_2$ | $C_{69}H_{70}B_2FeN_4O_3$ | $C_{38}H_{36}F_6FeN_8O_6S_2$ | $C_{84}H_{76}B_2FeN_8$ |
| fw | 767.52 | 644.35 | 1080.76 | 934.72 | 1275.00 |
| $T$, °C | −100 | −100 | −100 | −100 | 26 |
| $\lambda$, Å | 0.710 73 (Mo Kα) | 0.710 73 (Mo Kα) | 1.541 78 (Cu Kα) | 1.541 78 (Cu Kα) | 1.541 78 (Cu Kα) |
| space group, No. | $P2_1/n$, 14 | $P2_1/c$, 14 | $P2_1/n$, 14 | $Pc$, 7 | $P2_1/n$, 14 |
| $a$, Å | 12.418(2) | 17.636(2) | 17.525(1) | 10.236(1) | 12.489(1) |
| $b$, Å | 16.192(4) | 9.659(1) | 19.150(2) | 10.129(1) | 14.189(1) |
| $c$, Å | 15.855(2) | 16.004(2) | 17.703(1) | 19.251(1) | 19.843(1) |
| $\beta$, deg | 92.09(2) | 113.29(1) | 100.36(1) | 92.27(1) | 102.84(1) |
| $V$, Å$^3$ | 3185.8(10) | 2504.1(5) | 5844.3(8) | 1994.4(3) | 3428.4(4) |
| $Z$ | 4 | 4 | 4 | 2 | 2 |
| $\rho_{calcd}$, g cm$^{-3}$ | 1.600 | 1.709 | 1.228 | 1.557 | 1.235 |
| $\mu$, cm$^{-1}$ | 6.92 | 8.59 | 24.60 | 47.71 | 21.62 |
| $R^a$ | 0.0441 | 0.0392 | 0.0787 | 0.0464 | 0.0494 |
| $R_w{}^b$ | 0.1044 | 0.1036 | 0.1818 | 0.1173 | 0.1090 |

$^a$ $R = \sum||F_o| - |F_c||/\sum|F_o|$. $^b$ $R_w = [\sum w(F_o^2 - F_c^2)^2/\sum w(F_o^2)^2]^{1/2}$.

**Table 2.** Selected Bond Distances (Å) and Bond Angles (deg) for **1**-OTf·$CH_3CN$ and **1**-$BPh_4$

| | **1**-OTf·$CH_3CN$ | **1**-$BPh_4$ |
|---|---|---|
| Fe−N(1) | 1.978(3) | 1.993(7) |
| Fe−N(2) | 1.953(3) | 1.944(6) |
| Fe−N(3) | 1.959(3) | 1.986(8) |
| Fe−N(4) | 1.962(3) | 1.984(9) |
| Fe−N(5) | 1.934(3) | 1.941(7) |
| Fe−N(6) | 1.947(3) | 1.941(7) |
| N(1)−Fe−N(2) | 85.70(10) | 85.4(3) |
| N(1)−Fe−N(3) | 83.20(10) | 82.7(4) |
| N(1)−Fe−N(4) | 83.61(11) | 83.7(4) |
| N(2)−Fe−N(3) | 87.90(10) | 87.3(3) |
| N(2)−Fe−N(4) | 91.62(11) | 90.1(3) |
| N(3)−Fe−N(4) | 166.80(11) | 166.3(3) |
| N(1)−Fe−N(5) | 178.64(11) | 178.1(4) |
| N(1)−Fe−N(6) | 92.54(10) | 93.1(3) |
| N(2)−Fe−N(5) | 94.71(11) | 94.5(3) |
| N(2)−Fe−N(6) | 178.23(11) | 178.3(4) |
| N(3)−Fe−N(5) | 95.52(11) | 95.4(3) |
| N(3)−Fe−N(6) | 92.12(11) | 91.6(3) |
| N(4)−Fe−N(5) | 97.66(11) | 98.2(3) |
| N(4)−Fe−N(6) | 87.95(11) | 90.7(3) |
| N(5)−Fe−N(6) | 87.05(11) | 86.9(3) |

**Table 3.** Selected Bond Distances (Å) and Bond Angles (deg) for **2** and **3**·$CH_3OH$

| | | **2** | | **3**·$CH_3OH$ |
|---|---|---|---|---|
| Fe−N(1) | | 2.203(2) | | 2.198(6) |
| Fe−N(2) | | 2.179(2) | | 2.175(6) |
| Fe−N(3) | | 2.156(2) | | 2.145(6) |
| Fe−N(4) | | 2.174(2) | | 2.157(6) |
| Fe−O(1) | | 2.054(2) | | 2.039(5) |
| Fe−O | O(4) | 2.150(2) | O(2) | 2.194(5) |
| N(1)−Fe−N(2) | | 79.44(8) | | 79.8(2) |
| N(1)−Fe−N(3) | | 78.26(8) | | 77.3(2) |
| N(1)−Fe−N(4) | | 75.79(8) | | 77.5(2) |
| N(2)−Fe−N(3) | | 82.59(8) | | 93.6(2) |
| N(2)−Fe−N(4) | | 97.96(8) | | 84.1(2) |
| N(3)−Fe−N(4) | | 153.46(8) | | 154.7(2) |
| N(1)−Fe−O(1) | | 170.09(8) | | 175.6(2) |
| N(1)−Fe−O | O(4) | 96.80(8) | O(2) | 90.4(2) |
| N(2)−Fe−O(1) | | 91.04(8) | | 96.2(2) |
| N(2)−Fe−O | O(4) | 174.66(8) | O(2) | 168.9(2) |
| N(3)−Fe−O(1) | | 97.94(9) | | 101.1(2) |
| N(3)−Fe−O | O(4) | 92.96(7) | O(2) | 89.3(2) |
| N(4)−Fe−O(1) | | 108.56(9) | | 104.2(2) |
| N(4)−Fe−O | O(4) | 84.69(7) | O(2) | 88.8(2) |
| O(1)−Fe−O | O(4) | 92.51(8) | O(2) | 93.8(2) |

superglue on the end of a glass fiber. The diffraction intensities were collected using Mo Kα graphite-monochromated radiation ($\lambda$ = 0.710 73 Å) on a Siemens P4 single-crystal X-ray diffractometer (**1**-OTf·$CH_3CN$, **2**) or on a Siemens P4/RA single-crystal X-ray diffractometer with Cu Kα graphite-monochromated radiation ($\lambda$ = 1.541 78 Å) (**1**-$BPh_4$, **3**·$CH_3OH$, **4**-OTf, **4**-$BPh_4$). During data collection, the intensities of three representative reflections were monitored every 97 reflections, but in no case was any serious decay observed. The structures were solved either by direct methods or by Patterson interpretation and expansion (SHELXS-86) and difference Fourier methods, and they were refined by full-matrix least-squares methods (SHELXTL). All atoms in the coordination sphere were refined anisotropically. Hydrogen atoms were included and placed at calculated positions with C−H bond distances fixed at 0.96 Å. The details of the data collection and refinement procedures are given in Table 1 and in the CIF files. Selected bond lengths and angles are given in Tables 2−4.

## Results and Discussion

**Syntheses of Iron(II) Complexes.** Scheme 1 depicts the variety of complexes that can be prepared from iron(II) triflate and 1 or 2 equiv of TPA, depending on the stoichiometry and the nature of solvent and anions used. Iron(II) triflate is a particularly useful reagent because it can be easily prepared in a soluble, solvated form from iron powder and triflic acid in a variety of solvents.[19] It is air stable, can easily be made anhydrous, contains a weakly coordinating anion, and is a safe substitute for the perchlorate salt. The nitrogen donor atoms of the complexes reported here are provided by the tripodal potentially tetradentate ligand tris(2-pyridylmethyl)amine (TPA), which has served as a good model for the arrangement of the histidine groups anchoring the metal centers in many metalloproteins. In 1:1 complexes of Fe and TPA, six-coordinate complexes are favored and the remaining two coordination sites can be occupied by anions or neutral solvent molecules, depending on the conditions of synthesis.

In acetonitrile, the red, six-coordinate, LS complex [Fe(TPA)$(CH_3CN)_2$]$(SO_3CF_3)_2$ (**1**-OTf) was readily synthesized by adding 1 equiv of $Fe(SO_3CF_3)_2$·$2CH_3CN$ to 1 equiv of TPA under a dinitrogen atmosphere (eq 1). The presence of the two terminal organonitrile ligands was confirmed from an X-ray crystal structure study. Complex **1**-OTf readily loses its acetonitrile ligands when dissolved in noncoordinating solvents such as acetone or chloroform to afford yellow-orange solutions. Upon precipitation with pentane, the yellow-orange, HS complex Fe(TPA)$(SO_3CF_3)_2$ (**2**), in which the triflate anions are bound, forms (eq 2). This transformation is easily reversed by dissolving **2** in acetonitrile. By taking advantage of the lower solubility of the salt of a noncoordinating anion, $BPh_4^-$, we could prepare the pale orange, HS, methanol-bound complex [Fe(TPA)$(CH_3OH)_2$]$(BPh_4)_2$ (**3**). This complex was isolated

**Table 4.** Selected Bond Distances (Å) and Bond Angles (deg) for **4**-OTf and **4**-$BPh_4$

| | | **4**-OTf | | **4**-$BPh_4$ |
|---|---|---|---|---|
| Fe−$N_{amine}$ | N(1) | 2.330(5) | N(1) | 2.389(3) |
| | N(5) | 2.317(5) | N(1A) | 2.389(3) |
| Fe−$N_{pyridine}$ | N(2) | 2.149(5) | N(2) | 2.426(3) |
| | N(3) | 2.191(5) | N(3) | 2.482(3) |
| | N(4) | | N(4) | 2.540(3) |
| | N(6) | 2.215(5) | N(2A) | 2.426(3) |
| | N(7) | 2.134(5) | N(3A) | 2.482(3) |
| | N(8) | | N(4A) | 2.540(3) |
| N(1)−Fe−N(2) | | 75.7(2) | | 67.98(9) |
| N(1)−Fe−N(3) | | 73.1(2) | | 67.32(9) |
| N(1)−Fe−N(4) | | | | 66.41(9) |
| N(1)−Fe−N | N(5) | 117.0(2) | N(1A) | 180.0 |
| N(1)−Fe−N | N(6) | 92.7(2) | N(2A) | 112.02(9) |
| N(1)−Fe−N | N(7) | 163.1(2) | N(3A) | 112.68(9) |
| N(1)−Fe−N | | | N(4A) | 113.59(9) |
| N(2)−Fe−N(3) | | 107.7(2) | | 104.67(9) |
| N(2)−Fe−N(4) | | | | 107.09(9) |
| N(2)−Fe−N | N(5) | 159.6(2) | N(1A) | 112.02(9) |
| N(2)−Fe−N | N(6) | 92.7(2) | N(2A) | 180.0 |
| N(2)−Fe−N | N(7) | 96.3(2) | N(3A) | 75.33(9) |
| N(2)−Fe−N | | | N(4A) | 72.91(9) |
| N(3)−Fe−N(4) | | | | 106.17(9) |
| N(3)−Fe−N | N(5) | 91.8(2) | N(1A) | 112.68(9) |
| N(3)−Fe−N | N(6) | 150.8(2) | N(2A) | 75.33(9) |
| N(3)−Fe−N | N(7) | 95.9(2) | N(3A) | 180.0 |
| N(3)−Fe−N | | | N(4A) | 73.83(9) |
| N(4)−Fe−N | | | N(1A) | 113.59(9) |
| N(4)−Fe−N | | | N(2A) | 72.91(9) |
| N(4)−Fe−N | | | N(3A) | 73.83(9) |
| N(4)−Fe−N | | | N(4A) | 180.0 |
| N(5)−Fe−N(6) | | 71.7(2) | | |
| N(5)−Fe−N(7) | | 75.2(2) | | |
| N(6)−Fe−N(7) | | 102.6(2) | | |
| N(1A)−Fe−N(2A) | | | | 67.98(9) |
| N(1A)−Fe−N(3A) | | | | 67.32(9) |
| N(1A)−Fe−N(4A) | | | | 66.41(9) |
| N(2A)−Fe−N(3A) | | | | 104.67(9) |
| N(2A)−Fe−N(4A) | | | | 107.09(9) |
| N(3A)−Fe−N(4A) | | | | 106.17(9) |

when $NaBPh_4$ was added to a methanol solution containing 1 equiv each of $Fe(SO_3CF_3)_2 \cdot 2CH_3CN$ and TPA (eq 3). These two terminal methanol ligands are also easily displaced in solution: when **3** was dissolved in acetonitrile, an immediate color change from yellow to red was observed, and precipitation with diethyl ether resulted in the isolation in high yield of the red LS complex, $[Fe(TPA)(CH_3CN)_2](BPh_4)_2$ (**1**-$BPh_4$), an isostructural analog of complex **1**-OTf with tetraphenylborate as noncoordinating anions (eq 4).

Reaction in acetone of 2 equiv of TPA with $Fe(SO_3CF_3)_2 \cdot 2CH_3CN$ (eq 5) results in a mixture of **2** and a new iron(II) complex that can be crystallized in low yield from a yellow oil that forms in chloroform. The crystal structure has been solved and reveals a six-coordinate complex, $[Fe(TPA)_2](SO_3CF_3)_2$ (**4**-OTf). The low yield obtained was a consequence of the fact that complexes **4**-OTf and **2** exist as an equilibrium mixture in solution, with **4**-OTf easily losing a TPA ligand. A pure, colorless, eight-coordinate complex, $[Fe(TPA)_2](BPh_4)_2$ (**4**-$BPh_4$), was isolated instead when $NaBPh_4$ was added to a methanol solution of $Fe(SO_3CF_3)_2 \cdot 2CH_3CN$ and 2 equiv of TPA (eq 6). This complex also readily loses a TPA ligand when dissolved in acetonitrile (eq 7) to form red crystals of **1**-$BPh_4$, demonstrating the thermodynamic preference for the LS complex.

**Crystal Structures of Iron(II) Complexes.** A summary of crystal parameters and refinement results of all complexes (except **1**-$BPh_4$) is given in Table 1, and selected bond distances and angles appear in Tables 2−4. The molecular structures of the iron(II) complexes are shown in Figures 1−5.

**$[Fe(TPA)(CH_3CN)_2](SO_3CF_3)_2 \cdot CH_3CN$ (1-OTf·$CH_3CN$) and $[Fe(TPA)(CH_3CN)_2](BPh_4)_2$ (1-$BPh_4$).** X-ray diffraction studies showed that the two complexes, $[Fe(TPA)(CH_3CN)_2]^{2+}$ (**1**) in **1**-OTf·$CH_3CN$ and **1**-$BPh_4$, are isostructural. However, these complexes crystallize in different space groups owing to differences in the lattice solvent content and in the anions. The structure of **1** from **1**-OTf·$CH_3CN$ is depicted in Figure 1. Complex **1**-OTf crystallized as discrete cations and anions along with an acetonitrile solvate. In both compounds, the iron is coordinated to the four nitrogen atoms of TPA, and they adopt the characteristic configuration of such tripods, with $N_{amine}$−Fe−$N_{pyridine}$ angles averaging 84° to accommodate the five-membered chelate rings. Two *cis*-coordinated acetonitrile ligands complete the coordination sphere. The coordination of acetonitrile is nearly linear, with Fe−N−C angles of 174.9(3) and 175.1(3)° in **1**-OTf, and 171.5(9) and 173.2(8)° in **1**-$BPh_4$. The nearly octahedral $N_6$ environment around the irons is characterized by Fe−N distances of 1.934(3)−1.978(3) Å in **1**-OTf and 1.941(7)−1.993(7) Å in **1**-$BPh_4$, which are typical of LS iron(II).[27] These short Fe−N distances indicate that the TPA ligand and the nitrile groups are strongly coordinated to the Fe(II) center. This contrasts the HS iron(II) complexes **2** and **3** (*vide infra*), in which the Fe−N distances range from 2.156(2) to 2.203(2) Å in **2** and from 2.145(6) to 2.198(6) Å in **3**. The longest Fe−N distance involves the tertiary amine.

**$Fe(TPA)(SO_3CF_3)_2$ (2).** An ORTEP diagram of the structure is given in Figure 2. The asymmetric unit of this crystal structure contains a discrete mononuclear unit of the neutral complex, **2**. This molecule consists of one Fe(II) atom with the TPA ligand coordinated in a tripodal, tetradentate fashion, the two other coordination sites being occupied by terminally bonded triflates. The iron center is arranged in an approximate octahedral geometry with Fe−N distances ranging from 2.156(2) to 2.203(2) Å, which are characteristic of HS iron(II). The tertiary amine nitrogen is the weakest donor atom of TPA; hence, the Fe−$N_{amine}$ bond is longer than the Fe−$N_{pyridine}$ bonds, resulting in an asymmetry in the Fe−O distances. The shorter Fe−O(1) bond (2.054(2) Å) is for the triflate *trans* to the tertiary amine, and the longer Fe−O(4) bond (2.150(2) Å) is for the triflate *trans* to a pyridine. Such an asymmetry has also been observed in other TPA complexes containing a coordinated catecholate[28] or benzoylformate.[29]

**$[Fe(TPA)(CH_3OH)_2](BPh_4)_2 \cdot CH_3OH$ (3·$CH_3OH$).** The structure of the cationic portion of **3**·$CH_3OH$, $[Fe(TPA)(CH_3OH)_2]^{2+}$, is depicted in Figure 3. This structure has an asymmetric unit containing a discrete cation, two $BPh_4^-$ anions, and one molecule of lattice $CH_3OH$. The coordination sphere about the Fe(II) ion is a distorted octahedron with ligation from the tertiary amine and the three aromatic nitrogen atoms from the pendant pyridylmethyl arms of the TPA ligand. The fifth and sixth coordination sites are occupied by two methanol ligands. Both the Fe−$N_{amine}$ bond distance (2.198(6) Å) and the Fe−$N_{pyridine}$ bond distances (average 2.159(6) Å) are close to the corresponding distances found in compound **2** and are also characteristic of HS iron(II). The Fe−O distances are 2.039(5) Å for the methanol *trans* to the tertiary amine and 2.194(5) Å for the methanol *trans* to a pyridine. These bonds

(27) Butcher, R. J.; Addison, A. W. *Inorg. Chim. Acta* **1989**, *158*, 211−215.
(28) Jang, H. G.; Cox, D. D.; Que, L., Jr. *J. Am. Chem. Soc.* **1991**, *113*, 9200−9204.
(29) Chiou, Y. M.; Que, L., Jr. *J. Am. Chem. Soc.* **1995**, *117*, 3999−4013.

**Scheme 1**

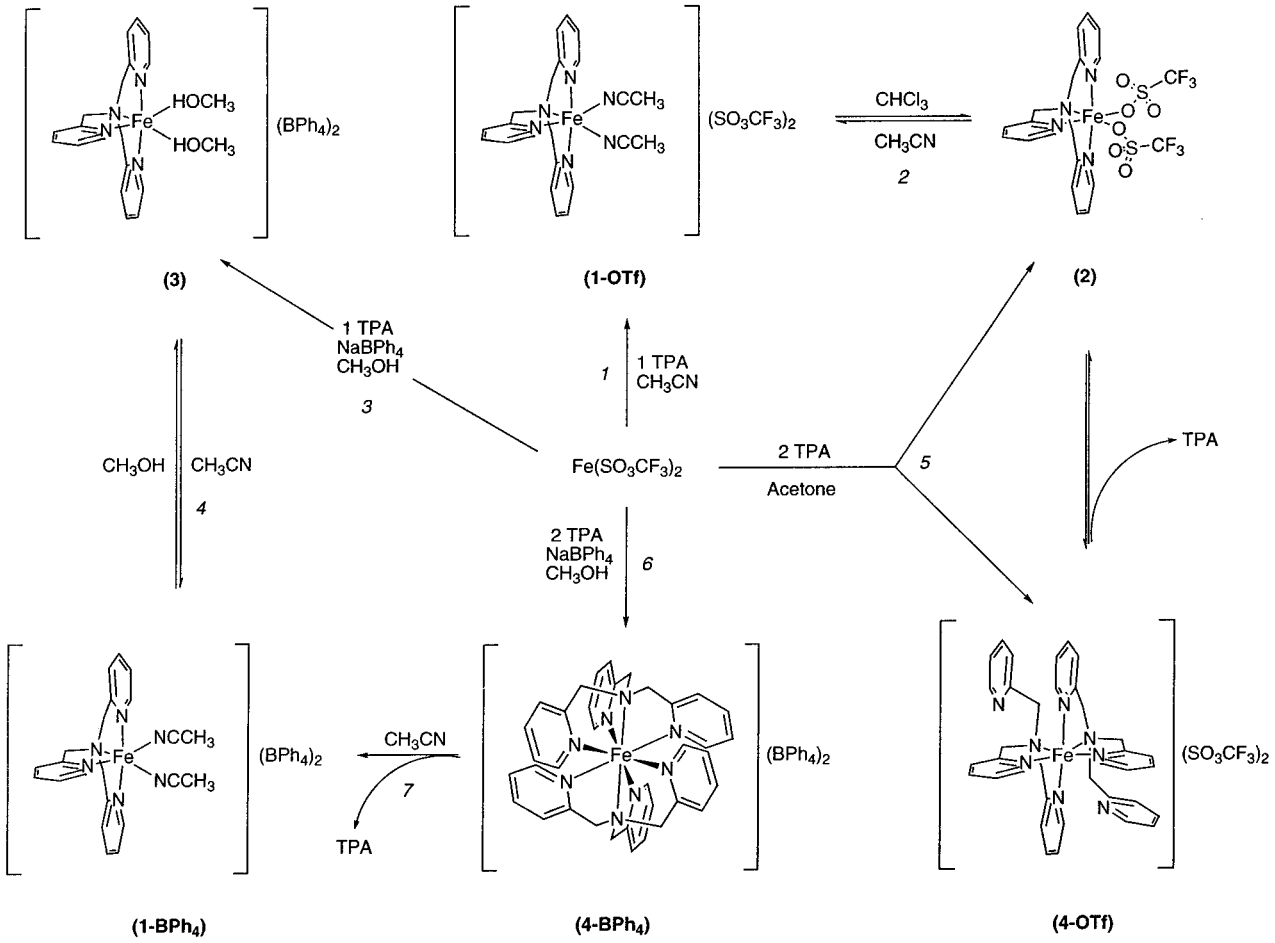


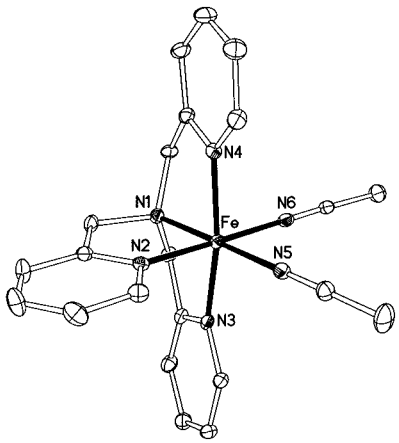


**Figure 1.** Molecular structure and atom-labeling scheme for $[Fe(TPA)(CH_3CN)_2]^{2+}$ (**1**-OTf) (30% thermal ellipsoids). Hydrogen atoms are omitted for clarity.

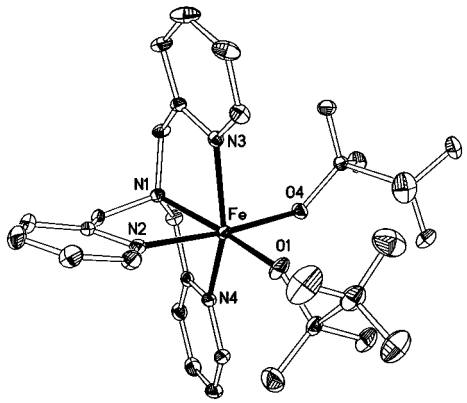


**Figure 2.** Molecular structure and atom-labeling scheme for $Fe(TPA)(SO_3CF_3)_2$ (**2**) (30% thermal ellipsoids). Hydrogen atoms are omitted for clarity.

to neutral oxygen donor ligands are remarkably similar to those to the weakly basic triflate anions in **2** and similar complexes.[28,29]

**$[Fe(TPA)_2](SO_3CF_3)_2$ (4-OTf).** A six-coordinate iron(II) complex (Figure 4) is obtained as the triflate salt with two TPA ligands each acting as a tridentate facial coordinating ligand with the two apical tertiary amines and two of the pyridylmethyl arms bound to the iron. The third pyridyl arm of each TPA remains uncoordinated. The structure has no crystallographically imposed symmetry yet adopts approximate $C_2$ symmetry with the tertiary amines located *cis* to each other. The Fe−$N_{amine}$ bond lengths of 2.330(5) and 2.317(5) Å are significantly longer than those observed in the other six-coordinate Fe(II)-TPA complexes, indicating that the aliphatic amine nitrogens bind only weakly to the iron ion. The Fe−$N_{pyridine}$ distances (Fe−N(3) = 2.191(5) Å, Fe−N(6) = 2.215(5) Å) are also slightly longer than those of the other related six-coordinate complexes where Fe−$N_{pyridine}$ = 2.134−2.179 Å. These differences may be a consequence of steric interactions between the $CH_2$ groups of the free pyridyl arms and two of the bound pyridine rings containing N(3) and N(6) (C(18)···N(6) = 3.094 Å, C(18)···C(19) = 3.351 Å, C(36)···N(3) = 3.147 Å, C(36)···C(7) = 3.342 Å). The presence of the five-membered chelate

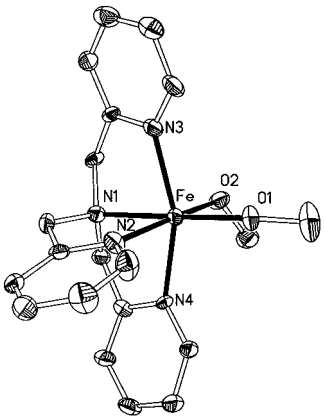


**Figure 3.** Molecular structure and atom-labeling scheme for $[Fe(TPA)(CH_3OH)_2]^{2+}$ (**3**) (30% thermal ellipsoids). Hydrogen atoms are omitted for clarity.

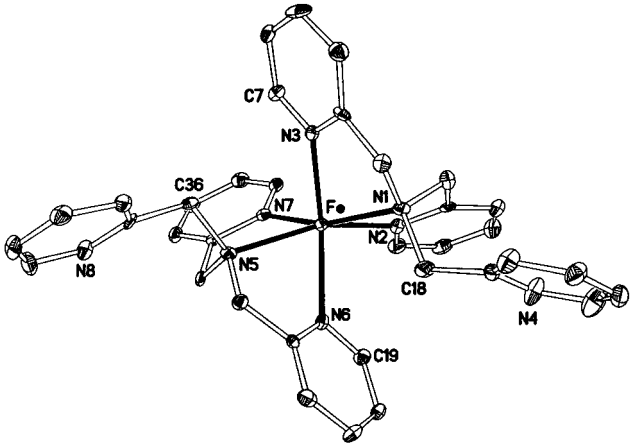


**Figure 4.** Molecular structure and atom-labeling scheme for $[Fe(TPA)_2]^{2+}$ (**4**-OTf) (30% thermal ellipsoids). Hydrogen atoms are omitted for clarity.

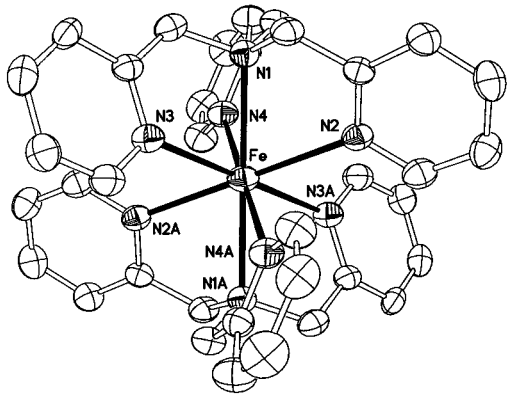


**Figure 5.** Molecular structure and atom-labeling scheme for $[Fe(TPA)_2]^{2+}$ (**4**-$BPh_4$) (30% thermal ellipsoids). Hydrogen atoms are omitted for clarity.

rings and the steric bulk of the $CH_2$ groups and long $Fe-N_{amine}$ bond lengths appear to be responsible for the extremely acute $N_{amine}-Fe-N_{pyridine}$ angles (73.1(2)° for N(1)−Fe−N(3), 75.7(2)° for N(1)−Fe−N(2), 71.7(2)° for N(5)−Fe−N(6), and 75.2(2)° for N(5)−Fe−N(7)) observed for this complex. A related octahedral iron(II) complex $[Fe(dpma)_2]^{2+}$ also adopts this $C_2$ symmetric structure with two *facial* coordinated tridentate nitrogen donor ligands and a *cis* arrangement of the two amines.[27] However, this unconstrained ligand affords the red, LS complex, as the $BF_4^-$, $Cl^-$, $Br^-$, or $NCS^-$ salt.[21] In contrast, the N-methylated ligand affords a HS complex, $[Fe(Medpma)_2]^{2+}$.[21] The two amine nitrogens have been linked in the hexadentate ligand tetrakis(2-pyridylmethyl)-1,2-ethanediamine, tpen, and related ligands[3] and form iron(II) complexes with similar geometry to **4**-OTf.

**$[Fe(TPA)_2](BPh_4)_2$ (4-$BPh_4$).** The structure of the dication $[Fe(TPA)_2]^{2+}$ from **4**-$BPh_4$ (Figure 5) shows an eight-coordinate iron ion at the center of a distorted cube, in which the eight ligating nitrogen atoms of two different ligand molecules occupy the corner positions. The stereochemistry of the six pyridyl nitrogens can also be described as forming the corners of a distorted octahedron (flattened) by 16° such that the N−Fe−N angles made by the pyridyl nitrogens on the same TPA molecule average 106° while that made by the *cis* pyridyl nitrogens on different TPA molecules average 74°. The amines then cap opposite faces of this distorted octahedron. The $N_{amine}-Fe-N_{pyridine}$ angles are 66.41(9)−67.98(9)° within a coordinated ligand molecule. The iron−nitrogen distances ($Fe-N_{amine}$ = 2.389(3) Å, $Fe-N_{pyridine}$ = 2.426(3)−2.540(3) Å) are significantly longer than those observed in the other six-coordinate Fe(II)−TPA complexes, resulting most likely from ligand steric crowding at the metal center. The N−Fe−N *trans* angles are all 180° as required by the inversion symmetry within **4**-$BPh_4$. A similar manganese(II) complex has been isolated as a perchlorate salt.[30] Complexes with coordination numbers exceeding 6 are uncommon for iron(II) and have generally been obtained with ligands having donor sets formed by nitrogen and oxygen atoms.[31,32] As far as we are aware, only four other eight-coordinate iron(II) complexes, in which all the donor nitrogens are part of chelating organic ligands, have been characterized structurally.[32]

**Magnetism in the Solid State and in Solution.** Solid-state and solution magnetic susceptibility measurements at room temperature have been determined for complexes **1**-OTf, **2**, and **4**-$BPh_4$. The magnetic moments are reported in Table 5. The magnetic moments at room temperature are 5.35 and 5.30 $\mu_B$ for complexes **2** and **4**-$BPh_4$, respectively, and are consistent with values expected for HS Fe(II) centers.[33] In contrast, complex **1**-OTf has a small residual magnetic moment ($\mu_{eff}$ = 0.86 $\mu_B$ at 297 K) that is typical of LS complexes.[4] This low effective moment value indicates that only a small amount HS population exists in the solid state at this temperature. The solution magnetic moments can be used to infer the molecular structure, especially with respect to ligand dissociation. In the case of $[Fe(TPA)]^{2+}$, the magnetic moment of complex **1**-OTf in $CD_3CN$ solution at 292.6 K is also 0.87 $\mu_B$, indicating that the solution structure is likely to be the same as in the crystal structure. However, a spin-crossover phenomenon for **1**-OTf in solution has been confirmed by observing a linear increase

(30) Gultneh, Y.; Farooq, A.; Karlin, K. D.; Liu, S.; Zubieta, J. *Inorg. Chim. Acta* **1993**, *211*, 171−175.
(31) (a) Meier, K.; Rihs, G. *Angew. Chem., Int. Ed. Engl.* **1985**, *24*, 858−859. (b) Drew, M. G. B.; Othman, A. H.; Nelson, S. M. *J. Chem. Soc., Dalton Trans.* **1976**, 1394−1399. (c) Drew, M. G. B.; Othman, A. H.; McIlroy, P.; Nelson, S. M. *Acta Crystallogr.* **1976**, *B32*, 1029−1031. (d) Beer, P. D.; Drew, M. G. B.; Leeson, P. B.; Ogden, M. I. *J. Chem. Soc., Dalton Trans.* **1995**, 1273−1283.
(32) (a) Di Vaira, M.; Mani, F.; Stoppioni, P. *J. Chem. Soc., Dalton Trans.* **1992**, 1127−1130. (b) Sakuta, M.; Hagen, K. S. *Abstracts of Papers*, 201st National Meeting of the American Chemical Society, Atlanta, GA, 1991; American Chemical Society: Washington, DC, 1991; INOR 230. (c) Singh, P.; Clearfield, A.; Bernal, I. *J. Coord. Chem.* **1971**, *1*, 29−37. (d) Koch, W. O.; Barbieri, A.; Grodzicki, M.; Schünemann, V.; Trautwein, A. X.; Krüger, H. J. *Angew. Chem., Int. Ed. Engl.* **1996**, *35*, 422−424.
(33) Hawker, P. N.; Twigg, M. V. In *Comprehensive Coordination Chemistry*; Wilkinson, G., Guillard, R. D., McCleverty, J. A., Eds.; Pergamon Press: New York, 1987; Vol. 4, pp 1213−1214.

**Table 5.** UV−Vis Absorption Properties, Effective Magnetic Moments, and $^1$H NMR Parameters of the Complexes

| | | | | $^1$H NMR[e] | | | | |
|---|---|---|---|---|---|---|---|---|
| complex | state | $\lambda_{max}$[b] ($\epsilon$[c]) | $\mu_{eff}$[d] ($\mu_B$) | py α | py $\beta$ | py $\beta'$ | py $\gamma$ | $CH_2$ |
| **1**-OTf | solid[a] | 409, 512 | 0.86 | | | | | |
| | $CH_3CN$ | 367 sh, 399 (8611), 516 (189) | 0.87[f] | 12.12[f] | 9.02 | 8.92 | 7.33 | 7.09 |
| **1**-$BPh_4$ | $CH_3CN$ | 367 sh, 397 (12475), 516 (269) | | 10.91[f] | 8.42 | 8.39 | *i* | 6.26 |
| **2** | solid[a] | 376, 1062 | 5.35 | | | | | |
| | $CHCl_3$ | 326 sh, 386 (1635), 931 (17) | 5.41[g] | 133.83[g] | 51.97 | 49.91 | 13.40 | 62.12 |
| **3** | acetone | 491 (187), 914 (12) | | 123.51[h] | 54.78 | 53.51 | 5.54 | 69.35 |
| **4**-OTf | acetone | 383 (1440), 901 (24) | | 73.83[h] | 41.26 | 41.26 | *j* | 30.59 |
| **4**-$BPh_4$ | solid[a] | 352 | 5.30 | | | | | |
| | acetone | 384 (1361), 502 sh, 894 (17) | 3.52[h] | 74.48[h] | 41.75 | 41.75 | 0.29 | 30.53 |

[a] Solid-state spectra measured by diffuse reflectance. [b] Units of nm. [c] Units of $M^{-1}$ $cm^{-1}$. [d] $T = 297$ K for solid-state measurements; $T = 293$ K for solution measurements (by Evans method). [e] $T = 293$ K. [f] In $CD_3CN$. [g] In $CDCl_3$. [h] In $(CD_3)_2CO$. [i] This peak overlaps with $BPh_4^-$ protons. [j] Not resolved from the TMS resonance.

in magnetic moment from 0.87 to 2.81 $\mu_B$ as the temperature is raised from 292.6 to 348 K. The temperature-induced LS ↔ HS equilibrium in other iron(II) TPA complexes has been demonstrated.[34] In this case, the spin crossover may be a conventional redistribution of population levels of LS and HS forms of **1**-OTf, or it may be a ligand substitution equilibrium between **1**-OTf and **2** in which one or more of the bound $CH_3CN$ ligands is displaced by a triflate at elevated temperatures. Complex **2** has, in $CHCl_3$ solution at 292.6 K, a $\mu_{eff}$ of 5.41 $\mu_B$, which is close to the value observed in the solid state and confirms the presence of a HS Fe(II) ion.

The magnetic moment of complex **4**-$BPh_4$ in acetone solution at 292.7 K is 3.52 $\mu_B$, which is much lower than the solid-state value of 5.30 $\mu_B$. The reason for this difference might come from a change of stereochemistry around the iron. Indeed, we have observed that, in solution, complex **4**-$BPh_4$ converts to a six-coordinate cation where a dynamic exchange of the bound and free pyridyl arms takes place (*vide infra*). In addition, a LS ↔ HS equilibrium behavior affords a diminished magnetic moment in solution.

**Solution Behavior According to $^1$H NMR.** The subtleties of solution behavior that are reflected in the solution magnetic moments are better analyzed by $^1$H NMR spectra in which isotropic shifts of ligand resonances are related to the bulk susceptibility of the solution and details of structure and bonding that affect the contact and dipolar contributions to the isotropic shifts. The $^1$H NMR spectra of the different iron(II) TPA complexes, recorded at ambient temperature in $CD_3CN$, $CDCl_3$, or $(CD_3)_2CO$, are presented in Figure 6 and Table 5. The general trend is for a downfield shift of the resonances when the iron(II) complexes are compared to the free ligand. The number of pyridine and methylene peaks observed shows that the TPA ligand has effective 3-fold symmetry in solution, suggesting that there is a facile exchange process that averages the environments of the three pendant pyridines on the time scale of the NMR experiment.

In deuterated acetonitrile, red LS complexes result (**1**-OTf and **1**-$BPh_4$). The $^1$H NMR spectra of these complexes show similar features, with well-separated signals due to the hydrogen atoms of the TPA ligand. In addition to the ligand resonances, the spectrum of complex **1**-$BPh_4$ exhibits the $BPh_4^-$ multiplets (7.20, 6.97, and 6.83 ppm) at the expected shifts. Although all the ligand resonances are downfield shifted, this phenomenon is most pronounced for the methylene protons and those occupying the α-position of the pyridine rings. The pyridine α protons, which are closest to the metal center, are assigned

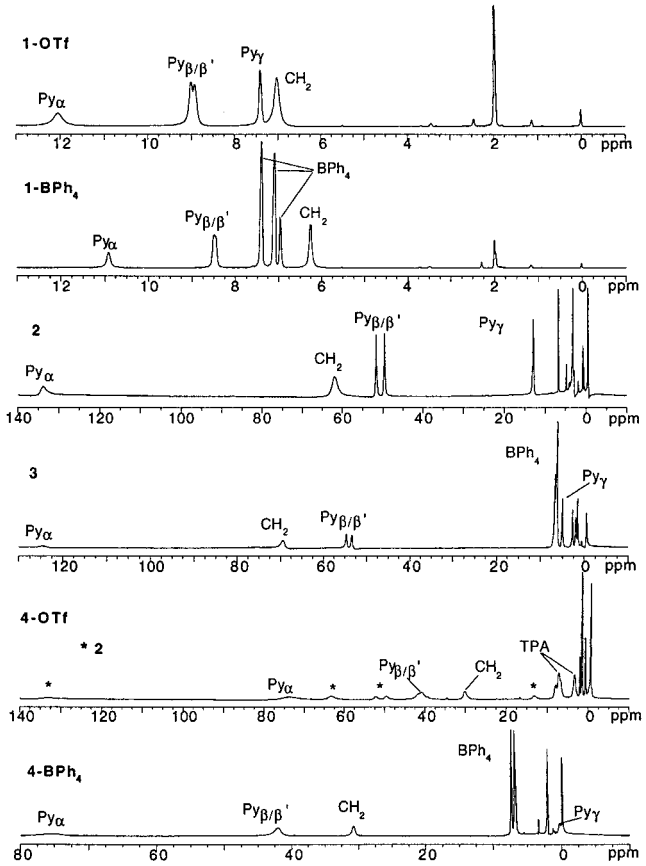


**Figure 6.** $^1$H NMR spectra of $[Fe(TPA)(CH_3CN)_2](SO_3CF_3)_2$ (**1**-OTf) (in $CD_3CN$), $[Fe(TPA)(CH_3CN)_2](BPh_4)_2$ (**1**-$BPh_4$) (in $CD_3CN$), $Fe(TPA)(SO_3CF_3)_2$ (**2**) (in $CDCl_3$), $[Fe(TPA)(CH_3OH)_2](BPh_4)_2$ (**3**) (in $(CD_3)_2CO$), $[Fe(TPA)_2](SO_3CF_3)_2$ (**4**-OTf) (in $(CD_3)_2CO$), and $[Fe(TPA)_2](BPh_4)_2$ (**4**-$BPh_4$) (in $(CD_3)_2CO$) at room temperature.

to the 12.12 (**1**-OTf) and 10.91 ppm (**1**-$BPh_4$) peaks due to their relative broadness, and the aliphatic protons from the methylene groups appear at 7.09 and 6.26 ppm, respectively, for **1**-OTf and **1**-$BPh_4$. The relatively large changes in chemical shift observed for the methylene and pyridine α protons (3.19 and 3.59 ppm (**1**-OTf) and 2.36 and 2.38 ppm (**1**-$BPh_4$), respectively, from the free ligand) probably result from their proximity to the nitrogen donor atoms; these protons would be expected to experience the strongest $\sigma$-donation effects. The remaining protons appear to behave similarly, although the chemical shift differences are not as large. The $\beta$ protons on each pyridine are resolved from each other and assigned to features at 9.02 and 8.92 ppm (**1**-OTf) and at 8.42 and 8.39 ppm (**1**-$BPh_4$). The pyridine $\gamma$ protons are found at 7.33 ppm in **1**-OTf, whereas in

(34) Højland, F.; Toftlund, H.; Yde-Andersen, S. *Acta Chem. Scand., Ser. A* **1983**, *37*, 251−257.

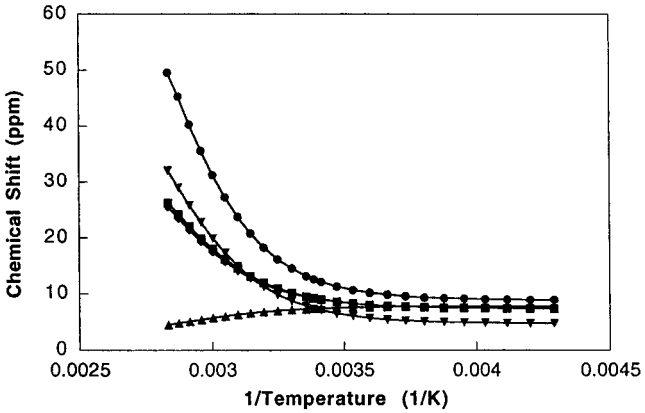


**Figure 7.** Plot of chemical shift versus $1/T$ for various resonances seen in the $^1$H NMR spectra of [Fe(TPA)(CH$_3$CN)$_2$](SO$_3$CF$_3$)$_2$ (**1**-OTf) in CD$_3$CN: (●) pyα; (■) py$\beta/\beta'$; (◆) py$\beta'/\beta$; (▲) py$\gamma$; (▼) CH$_2$.

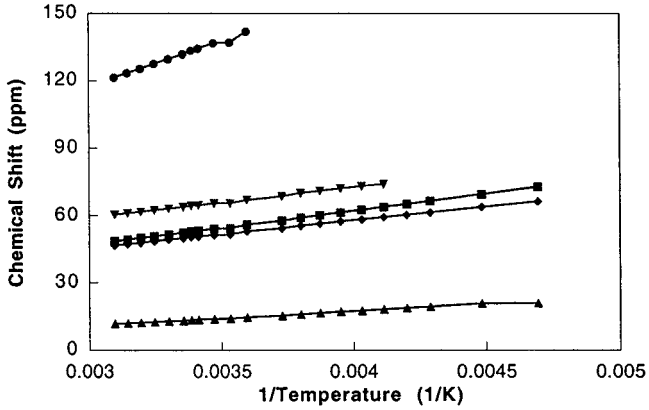


**Figure 8.** Plot of chemical shift versus $1/T$ for various resonances seen in the $^1$H NMR spectra of Fe(TPA)(SO$_3$CF$_3$)$_2$ (**2**) in (CD$_3$)$_2$CO: (●) pyα; (■) py$\beta/\beta'$; (◆) py$\beta'/\beta$; (▲) py$\gamma$; (▼) CH$_2$.

**1**-BPh$_4$, the resonance of these protons is masked by the intense BPh$_4^-$ multiplets.

$^1$H NMR spectra of **1**-OTf and **1**-BPh$_4$ in CD$_3$CN in the temperature range −40 to +80 °C were also recorded. A figure showing typical spectra is available in the Supporting Information. The results are summarized in Figure 7, where the chemical shifts of the various resonances are plotted versus inverse temperature. A pronounced deviation from Curie behavior due to the spin equilibrium is observed, confirming the temperature-induced LS ↔ HS equilibrium in **1**-OTf as observed by magnetic studies (*vide supra*). The shifts of **1**-OTf are greater than those of **1**-BPh$_4$, indicating that the dynamic exchanges that occur in solution to average the symmetry of the TPA ligands to near 3-fold symmetry may involve a transient coordination of the triflate ion.

On the other hand, when a noncoordinating solvent was used (CDCl$_3$ or (CD$_3$)$_2$CO), HS iron(II) complexes (**2** and **3**) were formed, as indicated by the large paramagnetic shifts observed in the corresponding $^1$H NMR spectra (cf. Figure 6). The large range in chemical shifts for these resonances is typical for HS iron(II) centers and resembles the spectra of the acetate-bridged dimer [Fe$_2$(OAc)$_2$(TPA)$_2$]$^{2+}$.[35] Furthermore, these spectra exhibit relatively sharp features for a paramagnetic complex, as expected from the short $T_1$ of a HS iron(II) center. All the resonances expected for these HS iron(II) TPA complexes are observed, including the signals belonging to the two BPh$_4^-$ counteranions present in **3**, and they are all well resolved. As in the LS complexes, the methylene protons and those occupying the α-position of the pyridine rings experience the largest deshielding effect. However, in these HS iron(II) complexes, the shifts are far downfield, indicating a predominance of $\sigma$-spin distributions. Indeed, the resonance corresponding to the α protons in **2** and **3** is found at 133.83 and 123.51 ppm, respectively, and that of the methylene protons at 62.12 (**2**) and 69.35 ppm (**3**). The $\beta$ protons also experience a large downfield shift with peaks at 51.97 and 49.91 ppm (**2**) and at 54.78 and 53.51 ppm (**3**). Finally, the $\gamma$ protons appear at 13.40 ppm for **2**, while they are upfield shifted at 5.54 ppm for **3**. A study of the temperature dependence of the chemical shifts of complex **2** in (CD$_3$)$_2$CO in the temperature range −60 to +50 °C was performed. A figure showing typical spectra is available in the Supporting Information. The results are summarized in Figure 8, where the chemical shifts of the various signals are plotted versus inverse temperature. The temperature dependence of these signals is in agreement with the Curie behavior. However, the temperature dependence of the protons occupying the α-position of the pyridine rings differs from those of the other protons. That of the α protons has a steeper slope. This difference may be attributed to the magnetic anisotropy of the HS iron(II) center, as well as to their proximity to the metal.

The $^1$H NMR spectrum of complex **4**-BPh$_4$ in (CD$_3$)$_2$CO at room temperature exhibits the BPh$_4^-$ multiplets (7.39, 6.91, and 6.73 ppm) and shows in addition four well-separated signals. Those of the pyridine α protons (74.48 ppm), $\beta$ protons (41.75 ppm), and methylene protons (30.53 ppm) are significantly downfield shifted, whereas the resonance for the $\gamma$ protons (0.29 ppm) is shifted upfield. The origin of the $^1$H resonance shifts described above depends on paramagnetic effects, due to the presence of the iron(II) in this complex. However, for **4**-BPh$_4$, the isotropic shifts are not as large as in the HS complexes **2** and **3**, indicating that the magnetic susceptibility of complex **4**-BPh$_4$ in solution could be lower than those for **2** and **3**. Magnetic susceptibility measurements in solution (Evans method) have confirmed this possibility (*vide supra*). These features indicated that, in solution, the eight-coordinate complex **4**-BPh$_4$ may be in equilibrium with a six-coordinate cation similar to the solid state structure of **4**-OTf. A dynamic exchange of the bound and free pyridyl arms affords an average structure with 3-fold symmetry. In addition, a LS ↔ HS equilibrium behavior decreases the chemical shifts of these resonances and affords a diminished magnetic moment in solution.

The $^1$H NMR spectrum of complex **4**-OTf in (CD$_3$)$_2$CO exhibits numerous isotropically shifted resonances in addition to those in the diamagnetic region. These peaks are accounted for by the presence of three species in solution (eq 5 of Scheme 1). The spectrum is consistent with an equilibrium mixture of **4**-OTf, **2**, and TPA in solution. The three relatively broad resonances observed for compound **4**-OTf are consistent with those observed for **4**-BPh$_4$. The pyridine α protons are assigned to the 73.83 ppm peak. The $\beta$ protons on each pyridine are not resolved from each other and are found at 41.26 ppm, and the methylene ligand protons appear at 30.59 ppm. The $\gamma$ proton resonance is probably not resolved from the TMS resonance. Although the triflate ion is considered to be a weakly coordinating ligand, its presence in solution dramatically alters the species present relative to the noncoordinating BPh$_4^-$ anion.

**UV−Vis−NIR Spectroscopy.** The colors of the complexes in the solid state vary from deep red for **1**-OTf and **1**-BPh$_4$ to yellow for **2**, **3**, and **4**-OTf and white-pale yellow for **4**-BPh$_4$.

(35) Menage, S.; Zang, Y.; Hendrich, M. P.; Que, L., Jr. *J. Am. Chem. Soc.* **1992**, *114*, 7786−7792.

Also, **1**-OTf shows, in solution in acetonitrile, a change in coloration on heating from room temperature to boiling temperature, going from deep red to orange. The electronic spectra of the complexes were recorded in solution and on solid samples (**1**-OTf, **2**, **4**-$BPh_4$). Absorption maxima are reported in Table 5. The intense higher energy transitions (326−400 nm) are found for all complexes in solution and are assigned as charge transfer transitions between the iron(II) ion and the pyridines.[36] The LS complexes have characteristic low-intensity d−d transitions at ∼516 nm. In the presence of a noncoordinating solvent ($CHCl_3$ or acetone), compounds **2** and **3** exhibit the typical yellow color for HS iron(II) TPA complexes,[37] and a broad lower energy band (931 and 914 nm, respectively, for **2** and **3**) was observed in the spectra, whose intensity is consistent with spin-allowed d−d transitions. The spectra of complexes **4**-OTf and **4**-$BPh_4$ in acetone present identical features (bands at 383 and 901 nm for **4**-OTf and at 384 and 894 nm for **4**-$BPh_4$), indicating that the stereochemistries around the Fe(II) in solution are likely the same. Indeed, we have observed that, in solution, complex **4**-$BPh_4$ converts to the six-coordinate cation seen in the structure of **4**-OTf (*vide supra*). This dynamic behavior could explain why crystals of **4**-$BPh_4$ are colorless, whereas in acetone, a pale yellow solution is observed. This situation should enhance the covalency of the iron−nitrogen bonds and lower the barrier for ligand to metal charge transfer as indicated by the low energy of the charge transfer band observed (384 nm). In the solid state, this charge transfer band appears at a higher energy. Furthermore, in acetonitrile, **4**-$BPh_4$ undergoes dissociation typical of eight-coordinate compounds. The resulting spectrum is very similar to that of **1**-$BPh_4$.

(36) Borovik, A. S.; Papaefthymiou, V.; Taylor, L. F.; Anderson, O. P.; Que, L., Jr. *J. Am. Chem. Soc.* **1989**, *111*, 6183−6195.

## Conclusions

The reaction system of $Fe^{2+}$ and TPA affords a number of species in solution and in the solid state, depending on the stoichiometry of the reaction, the solvent, and the counterion. The red LS complex forms in acetonitrile even in the presence of excess ligand, whereas in noncoordinating or weakly coordinating solvents yellow HS complexes form. In the presence of 2 equiv of TPA, either six-coordinate bis-TPA complexes or an eight-coordinate complex can be isolated. These bis-TPA iron(II) complexes exist in equilibrium with mono-TPA iron(II) complexes in solution when the triflate counterion is present but not when the counterion is $BPh_4^-$. These solution studies are a necessary prelude to understanding the reactivity of dioxygen with these complexes in their role as models of the active sites of non-heme proteins.

**Acknowledgment.** This work was supported by grants from the National Institutes of Health (GM 46506 and S10 RR07323).

**Supporting Information Available:** A plot of the effective magnetic moment of **1**-OTf in solution as a function of temperature (Figure S1) and variable-temperature $^1H$ NMR spectra for complexes **1**-OTf and **2** (Figures S2−S5) (5 pages). Six X-ray crystallographic files, in CIF format, are available on the Internet. Ordering and access information is given on any current masthead page.

IC971105E

(37) (a) Zang, Y.; Jang, H. G.; Chiou, Y. M.; Hendrich, M. P.; Que, L., Jr. *Inorg. Chim. Acta* **1993**, *213*, 41−48. (b) Ménage, S.; Zang, Y.; Hendrich, M. P.; Que, L., Jr. *J. Am. Chem. Soc.* **1992**, *114*, 7786−7792.